

# Experimental Demonstration of Quantum State Multi-meter and One-qubit Fingerprinting in a Single Quantum Device

Jiangfeng Du,<sup>1,2,\*</sup> Ping Zou,<sup>1</sup> Daniel K. L. Oi,<sup>3</sup> Xinhua Peng,<sup>4</sup> L.C.Kwek,<sup>5</sup> C.H. Oh,<sup>2</sup> and Artur Ekert<sup>3</sup>

<sup>1</sup>Hefei National Laboratory for Physical Sciences at Microscale and Department of Modern Physics, University of Science and Technology of China, Hefei, Anhui 230026, P.R. China

<sup>2</sup>Department of Physics, National University of Singapore, 117542 Singapore

<sup>3</sup>Centre for Quantum Computation, DAMTP, University of Cambridge, Wilberforce Road, Cambridge CB3 0WA, U.K.

<sup>4</sup>Universität Dortmund, Fachbereich Physik, 44221 Dortmund, Germany

<sup>5</sup>Department of Natural Sciences, National Institute of Education, Nanyang Technological University, 1 Nanyang Walk, Singapore 637616.

We experimentally demonstrate in NMR a quantum interferometric multi-meter for extracting certain properties of unknown quantum states without resource to quantum tomography. It can perform direct state determinations, eigenvalue/eigenvector estimations, purity tests of a quantum system, as well as the overlap of any two unknown quantum states. Using the same device, we also demonstrate one-qubit quantum fingerprinting.

PACS numbers: 03.67.Lx, 82.56.-b

Quantum information processors exploit the quantum features of superposition and entanglement for applications not possible in classical devices, offering the potential for significant improvements in the communication and processing of information. Many quantum circuits have been developed for quantum information processing, both for efficient algorithms and for secure communication. Of these, a versatile circuit is the so-called ‘scattering’ circuit [1, 2, 3, 4, 5, 6, 7]. Versions of this circuit play a crucial role in many quantum algorithms exhibiting marked improvements over the best classical counterparts. For example, it occurs in Kitaev’s solution to the Abelian stabilizer problem [1], in the analysis of quantum algorithms [2], for finding approximate eigenvalues of certain Hamiltonians [3], demonstrating tomography and spectroscopy as dual forms of quantum computation [5], quantum fingerprinting [5], direct estimations of linear and nonlinear functions of a quantum state [6], as well as direct detection of quantum entanglement[7].

Correspondingly, much effort has been made to physically realize quantum devices in many different physical systems. Nuclear magnetic resonance (NMR) has been the first to demonstrate non-trivial quantum algorithms with small numbers of qubits [8]. In this letter, we demonstrate the experimental implementation of the above quantum device using three qubits and nuclear magnetic resonance (NMR) techniques. We demonstrate its application to direct state determination and eigenvalue/eigenvector estimation of unknown qubit states, estimation of the overlap of any two states, and the implementation of a qubit fingerprinting scheme [9].

The network of the quantum device is shown in Fig.1. The Hadamard gate ( $H$ ) maps  $|b\rangle \mapsto \frac{1}{\sqrt{2}}(|0\rangle + (-1)^b|1\rangle)$ ,  $b \in \{0,1\}$ , and the phase shift gate  $\varphi =$

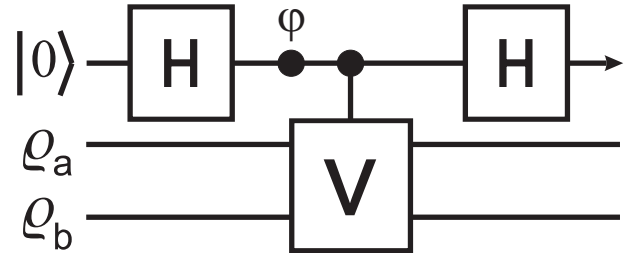


FIG. 1: The ‘Scattering Circuit’. The top line represents an ancilla qubit, initialised in the state  $|0\rangle$ , acting as a “probe particle”. The lower two lines represent two physical systems of interest. A controlled- $V$  operation is applied between two Hadamard gates and a phase shift gate. A measurement of the probe in the  $\{0,1\}$  basis reveals the overlap of the two input states.

$e^{-i\varphi\sigma_z/2}$  rotates the qubit by the angle  $\varphi$  about the  $z$  axis. The controlled- $V$  gate is the controlled-SWAP gate (also called quantum Fredkin gate), which acts trivially if the control qubit is in state  $|0\rangle$  and swaps the states of the lower systems if the control qubit is in the state  $|1\rangle$ , where  $V|\alpha\rangle_a|\beta\rangle_b = |\beta\rangle_a|\alpha\rangle_b$  for all pure states  $|\alpha\rangle$  and  $|\beta\rangle$ . With general two input states  $\rho_a$  and  $\rho_b$ , the reduced density matrix of the ancilla qubit at the end will have the form

$$\begin{pmatrix} \frac{1}{2}(1 + \cos \varphi \text{Tr}[\rho_a \rho_b]) & \frac{1}{2}i \sin \varphi \text{Tr}[\rho_a \rho_b] \\ -\frac{1}{2}i \sin \varphi \text{Tr}[\rho_a \rho_b] & \frac{1}{2}(1 - \cos \varphi \text{Tr}[\rho_a \rho_b]) \end{pmatrix}. \quad (1)$$

The probabilities of measuring the ancilla qubit are  $P_0 = \frac{1}{2}(1 + \cos \varphi \text{Tr}[\rho_a \rho_b])$  in state  $|0\rangle$  and  $P_1 = \frac{1}{2}(1 - \cos \varphi \text{Tr}[\rho_a \rho_b])$  in state  $|1\rangle$ . The difference of these two probabilities is  $|P_0 - P_1| = |\cos \varphi \text{Tr}[\rho_a \rho_b]|$ , which can easily be measured on the NMR interferometer. With  $\varphi = 0$ , it is the visibility  $v = \text{Tr}[\rho_a \rho_b]$ .

We implemented the circuit in liquid-state NMR using as qubits the three spin- $\frac{1}{2}$  carbon nuclei in a  $^{13}\text{C}$ -labeled sample of alanine  $\text{NH}_3^+ - \text{C}^\alpha \text{H}(\text{C}^\beta \text{H}_3) - \text{C}'\text{OOH}$

\*Electronic address: djf@ustc.edu.cn

in deuterated water.  $C'$  forms the ancilla system which is denoted as control qubit-1,  $C^\alpha$  and  $C^\beta$  form the target systems that are denoted as qubit-2 and qubit-3 (top, middle and bottom lines in Fig.1). With decoupling of the protons, this spin system exhibits a weakly coupled spectrum corresponding to the Hamiltonian  $H = \sum_{i=1}^3 \omega_i \frac{\sigma_z^i}{2} + \frac{\pi}{2} (J_{i,i+1} \sigma_x^i \sigma_z^{i+1})$  where  $\sigma_k$  are rescaled Pauli matrices,  $\frac{\omega_i}{2\pi}$  are Larmor frequencies and  $J_{ij}$  are spin-spin coupling constants. The experiments were carried out at the National Institute of Sciences of Nanyang Technological University on a Bruker Avance *DMX400* spectrometer in a field of roughly  $9.4T$  equipped with a  $5mm$  probe. The frequency shifts of the other carbons with respect to the third are  $12609.6Hz$  for the first and  $-3455.7Hz$  for the second, while the coupling constants are  $J_{12} = -1.2Hz$ ,  $J_{23} = 35Hz$ , and  $J_{13} = 54Hz$ . Longitudinal relaxation times ( $T_1$ ) for all three spins exceeded  $1.5s$ , while the transverse relaxation times ( $T_2$ ) were at least  $420ms$ .

Experimentally, the whole process of the device is demonstrated in three steps:

(1) Prepare the input state  $|0\rangle\langle 0| \otimes \rho_a \otimes \rho_b$ : As is standard, the density matrix of a spin- $\frac{1}{2}$  particle can be written in terms of the Bloch vector  $\vec{r}$  and the Pauli matrices  $\vec{\sigma} = \{\sigma_x, \sigma_y, \sigma_z\}$  as  $\rho = \frac{1}{2} (I + \vec{r} \cdot \vec{\sigma})$  (where  $I$  is the unit matrix). The length of the Bloch vector  $r$  gives a measure of purity (pure  $r = 1$  to maximally mixed  $r = 1$ ). In our experiments, we first use the spatial labelling method [10] to prepare the effective pure state  $\rho_{pp} = |000\rangle\langle 000| = \frac{(I+\sigma_z^1)}{2} \otimes \frac{(I+\sigma_z^2)}{2} \otimes \frac{(I+\sigma_z^3)}{2}$ . To prepare arbitrary mixed states  $\rho_a$  and  $\rho_b$  from  $\rho_{pp}$ , we adopt the similar method in previous experiments where both unitary operators and non-unitary operators are used [11].

For example, to create the mixed states  $\rho_a \otimes \rho_b = \left(\frac{I}{2} + \frac{\sqrt{2}}{2}\sigma_z^2\right) \otimes \left(\frac{I}{2} + \frac{1}{2}\sigma_x^3\right)$  from  $\rho_{pp}$ , two spin-selective radio frequency (RF) pulses,  $e^{-i\frac{\pi}{8}\sigma_x^2}$  and  $e^{-i\frac{\pi}{8}\sigma_x^3}$ , are applied on qubit-2 and qubit-3 respectively. They transform  $\frac{(I+\sigma_z^2)}{2} \otimes \frac{(I+\sigma_z^3)}{2}$  to the state  $\left(\frac{I}{2} - \frac{\sqrt{2}}{2}\sigma_y^2 + \frac{\sqrt{2}}{2}\sigma_z^2\right) \otimes \left(\frac{I}{2} - \frac{\sqrt{3}}{2}\sigma_y^3 + \frac{1}{2}\sigma_z^3\right)$ . A pulsed field gradient (PFG) in  $z$ -direction is then applied to dephase off-diagonal elements of the density matrix leading the state  $\left(\frac{I}{2} + \frac{\sqrt{2}}{2}\sigma_z^2\right) \otimes \left(\frac{I}{2} + \frac{1}{2}\sigma_z^3\right)$ . Finally, by applying another spin selective RF pulse  $e^{-i\frac{\pi}{4}\sigma_y^3}$ , the desired state is prepared. Therefore, the Bloch lengths of spin 2 and 3 have been shortened to purities  $r_a = \frac{\sqrt{2}}{2}$  and  $r_b = \frac{\sqrt{3}}{2}$  by non-unitary operations, while the orientation of the spin vector has been rotated to the desired direction by unitary operations. Hence, we can generate the state of each spin with any length and orientation in the Bloch sphere. In the experiments, all the spin selective pulses are Gaussian-shaped and have the same pulse duration  $0.866ms$ , with the rotation magnitude determined by the pulse power.

(2) Application of the circuit: The single qubit gates  $H$  and  $\varphi$  gate are easily realized in NMR [8]. However,

it is difficult to directly realize the three-qubit Fredkin gate [12]. In principle, the gate can be decomposed into one and two-qubit gates [13]. Chau and Wilczek gave a construction using six specific gates [14], Smolin and DiVincenzo then showing that five two-qubit gates were optimal [15]. However, it is still difficult to realize the three-qubit Fredkin gate precisely in practice. In NMR, one efficient choice is to directly construct multi-qubit quantum gates by using low-power RF pulses on a single multiplet-component (transition-selective excitation or TSE). This takes advantage of the full complexity of the internal Hamiltonian and uses the scalar coupling between pairs of spins to construct multi-qubit logic gates, which operate on many qubits simultaneously [16].

We implement the circuit by the pulse sequence (left to the right)

$$R_\varphi^1\left(\frac{\pi}{2}\right) - TP1 - TP2 - TP3 - R_\delta^1\left(\frac{\pi}{2}\right), \quad (2)$$

where  $R_\varphi^1\left(\frac{\pi}{2}\right) = e^{-i\frac{\pi}{4}(\sigma_x \cos \varphi + \sigma_y \sin \varphi)}$  denotes a  $\pi/2$  selective pulse that acts on qubit-1 about the axis  $\hat{x} \cos \varphi + \hat{y} \sin \varphi$ , combining the first Hadamard and the  $\varphi$  gate in Fig. 1. The next three transition pulses perform a modified Fredkin gate which induces a nontrivial phase factor [17]. The duration of each Gaussian-shaped TSE pulses were  $73.5ms$  for sufficient selectivity in the frequency domain without disturbing the nearest line (see [18] for detailed analysis of TSE pulses).

(3) Measure the ‘‘probe’’ qubit-1. The final reduced density matrix of qubit-1 is

$$\begin{aligned} \rho_1 = \begin{pmatrix} \rho_{00} & \rho_{01} \\ \rho_{10} & \rho_{11} \end{pmatrix} &= (\rho_{01} + \rho_{10})\frac{\sigma_x^1}{2} + (\rho_{01} - \rho_{10})i\frac{\sigma_y^1}{2} \\ &+ (\rho_{00} - \rho_{11})\frac{\sigma_z^1}{2} + (\rho_{00} + \rho_{11})\frac{I}{2}. \end{aligned} \quad (3)$$

We will obtain the difference between the probabilities of finding qubit-1 in state  $|0\rangle$  and  $|1\rangle$  when the coefficient of  $\frac{\sigma_z^1}{2}$  is measured. We first apply a PFG to remove the non-diagonal part of the density matrix, then a pulse  $R_{\frac{\pi}{2}}^1\left(\frac{\pi}{2}\right)$ .

The state of qubit-1 is now  $(\rho_{00} - \rho_{11})\frac{\sigma_x^1}{2} + \frac{1}{2}(\rho_{00} + \rho_{11})I$ . Since the identity matrix in NMR is not observable, the integral area of peaks of qubit-1 is now proportional to  $(\rho_{00} - \rho_{11}) = \cos \varphi \text{Tr}[\rho_a \rho_b]$ . Practically, this is measured by integrating the entire multiplet and adding together the signals arising from the four components of qubit-1. Fig.2a compares interference patterns, from theory [6] and experiment, for both the pure and mixed states. Note that the additional phase factor induced by the three TSE pulses has no effect in testing the interference pattern since both the Bloch vectors of the inputs  $\rho_{a,b}$  are in the  $z$ -direction, the angle  $\delta$  of right pulse shown in Eq.(2) is set to  $\frac{\pi}{2}$ . It can be seen that the phase shift due to the SWAP operator is zero, and the visibility decreases when the input state changes from being pure ( $r = 1$ ) to mixed ( $r = \sqrt{3}/2$ ).

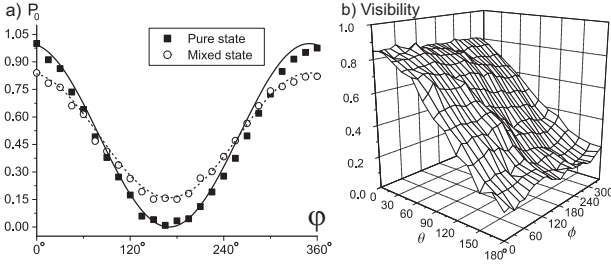


FIG. 2: a) The interference pattern for both pure and mixed state as function of the angle  $\varphi$  of phase gate. The boxes and circles are experimental results when both input states  $\{\varrho_a, \varrho_b\}$  are equal to  $\frac{I+\sigma_z}{2}$  or  $\frac{I}{2} + \frac{\sqrt{3}\sigma_z}{4}$  respectively. The solid and dotted curves correspond to the theoretical interference pattern  $P_0 = \frac{1}{2}(1 + \cos \varphi \cdot \text{Tr}[\varrho_a \varrho_b])$ . b) The experimental visibilities  $\text{Tr}[\varrho_a \varrho_b]$  measured when the pure state  $\varrho_a(\theta, \phi)$  is scanned over the Bloch sphere by changing the angle  $\theta$  and  $\phi$ . The second input state,  $\varrho_b$  is fixed as  $\varrho_b = \frac{I}{2} + \frac{\sqrt{2}\sigma_z}{4}$ .

We now implement a quantum multimeter and perform quantum fingerprinting using the circuit. A multimeter can be used to estimate the properties of a quantum state, or compare two quantum states, which are basic quantum processing tasks. Quantum fingerprinting is a proof-in-principle of an exponential quantum/classical gap for the equality problem in the simultaneous message passing model of communication complexity [5, 9, 19]. In both applications, to cancel the effect of the additional phase factor induced by three TSE pulses, we set the  $\varphi = \pi/4$  and  $\delta = 3\pi/2$  in Eq.(2).

*Multimeter for an unknown state:* We detect an unknown qubit state of  $\varrho_b$  and find its eigenvalue and eigenstate by using some particular known states as input state  $\varrho_a$ . We show below how this can be done by preparing suitable initial states  $\varrho_a$ .

We set input  $\varrho_b$  as the unknown state, and separately prepare three comparison states  $|\psi_a\rangle\langle\psi_a| \in \left\{ \frac{I+\hat{\sigma}_x}{2}, \frac{I+\hat{\sigma}_y}{2}, \frac{I+\hat{\sigma}_z}{2} \right\}$  as  $\varrho_a$ . Therefore the visibility of qubit-1 in each run contains information of the unknown state  $\varrho_b$ , which corresponds to the expectation value  $\langle\sigma_{bi}\rangle = \frac{1+r_{bi}}{2}$ ,  $i = \{x, y, z\}$ . Hence we can determine the density matrix  $\varrho_{\text{exp}}$  of the unknown state from these three values. Experimentally, we test many ‘‘unknown quantum’’ states, evaluating the performance using the Uhlmann fidelity [20],  $\mathcal{F}[\varrho_b, \varrho_{\text{exp}}] = \text{Tr}[\sqrt{\sqrt{\varrho_b}\varrho_{\text{exp}}\sqrt{\varrho_b}}]^2$ , which gave an average fidelity  $\mathcal{F}[\varrho_b, \varrho_{\text{exp}}] = 0.98 \pm 0.01$ .

By replacing above three states  $|\psi_a\rangle$ , we can estimate eigenvalues and eigenvectors of  $\varrho_b$ . We scan  $\varrho_a = \frac{I+\vec{r}_a\vec{\sigma}}{2}$ ,  $\vec{r}_a = (\cos\theta\cos\phi, \cos\theta\sin\phi, \sin\theta)$ , with  $\theta$  ranging from  $0^\circ$  to  $180^\circ$  in  $15^\circ$  steps, and  $\phi$  from  $0^\circ$  to  $345^\circ$  with  $15^\circ$  steps. We then measure  $\text{Tr}[\varrho_a\varrho_b]$ , and find the minimum and maximum. The two extrema are the eigenvalues of the unknown state  $\varrho_b$ , and the corresponding input states are its eigenvectors. Fig.2b shows the estimation of eigenvalues and eigenvectors of  $\varrho_b = \frac{I}{2} + \frac{\sqrt{2}\sigma_z}{4}$ . The

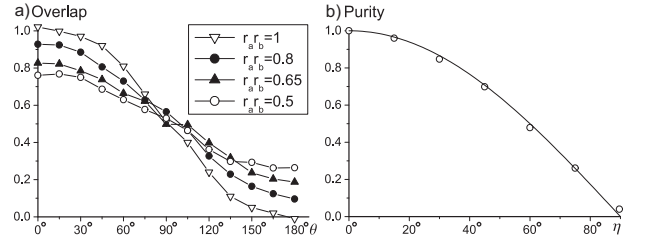


FIG. 3: a) Overlap as a function of  $\theta$ , the angle between state vectors, with different purities  $r_a$  and  $r_b$ . Four sets of experiments are shown in the figure, distinguished by different purities of the two states  $(r_a, r_b) = \{(1, 1), (1, 0.8), (0.81, 0.81), (1, 0.5)\}$ . b) Experimental determined purity as a function of  $\eta$ . The circles correspond to experimental results, and the curve corresponds to theory:  $r = \cos \eta$ .

experimentally determined eigenvalues are  $\{0.833, 0.182\}$  for eigenvectors  $|0\rangle$  and  $|1\rangle$  respectively, which compare well with the ideal results,  $\left\{\frac{1}{2} \pm \frac{\sqrt{2}}{4}\right\} = \{0.854, 0.146\}$ .

*Multimeter for two unknown states:* We can also compare two general quantum states. For pure states  $\varrho_a = |\alpha\rangle\langle\alpha|$  and  $\varrho_b = |\beta\rangle\langle\beta|$ , the visibility of qubit-1 gives  $\text{Tr}[\varrho_a\varrho_b] = |\langle\alpha|\beta\rangle|^2$ , i.e. the orthogonality of  $|\alpha\rangle$  and  $|\beta\rangle$ . For mixed states the visibility provides the measure of overlap  $\text{Tr}[\varrho_a\varrho_b]$  of  $\varrho_a$  and  $\varrho_b$ . If  $\varrho_a = \varrho_b = \varrho$  then  $\text{Tr}[\varrho_a\varrho_b] = \text{Tr}[\varrho]^2$ , which is the purity of  $\varrho$ .

We prepare various states  $\varrho_a$  and  $\varrho_b$  as the inputs, applying the circuit and measuring their corresponding visibilities, i.e., the overlap  $\text{Tr}[\varrho_a\varrho_b] = \frac{1+r_a r_b \cos\theta}{2}$ , where  $r_{a,b}$  are the lengths of the Bloch vectors  $\vec{r}_{a,b}$ , and  $\theta$  is the mutual angle between them. Fig.3a shows the experimental performance to compare the two unknown quantum states  $\varrho_a$  and  $\varrho_b$ . The device successfully gives the direct estimation of the overlap of two unknown states. Moreover, for two pure states, i.e.,  $r_a = r_b = 1$ , the experimental results present the direct measure of orthogonality.

We can also directly estimate the purity of a mixed state. We begin by preparing  $\varrho_a$  and  $\varrho_b$  in the same mixed state  $\frac{1}{2}(I + r\sigma_z)$ , where  $r = \cos\eta$  ( $\eta = \frac{n\pi}{12}$ ,  $n = 0, 1, \dots, 6$ ) is the purity. For each mixed state, the visibility  $\text{Tr}[\varrho^2] = \frac{1+r^2}{2}$  is measured from which  $r$  can easily be extracted (Fig.3b).

*Quantum Fingerprinting:* Finally, we demonstrate quantum fingerprinting [5], for which Beaudrap [9] recently defined and presented one-qubit versions which outperform any classical one-bit schemes. We implement the scheme from [9] as follows:

Alice and Bob use the same set of pure states  $\{|\phi_\sigma\rangle\}_{\sigma \in S}$  as fingerprints. In particular, we set  $|S| = 6$  and  $\{|\phi_\sigma\rangle\}_{\sigma \in S} = \{|\pm x\rangle, |\pm y\rangle, |\pm z\rangle\}$ . The absolute value of the inner product of any two distinct states does not exceed  $|\langle\alpha|\beta\rangle| \leq \delta = \frac{1}{\sqrt{2}}$ .

Alice and Bob send to a referee their fingerprints  $|\phi_\alpha\rangle$  and  $|\phi_\beta\rangle$  randomly selected from  $S$ . The referee then

needs to distinguish between the cases  $\alpha = \beta$  and  $\alpha \neq \beta$ . The referee puts the two states as the inputs  $\{\varrho_a, \varrho_b\}$  of the circuit, from which measurement of the first qubit gives the visibility  $\text{Tr}[\varrho_a \varrho_b] = |\langle \phi_\alpha | \phi_\beta \rangle|^2$ . From measurements of all 36 combinations, we obtain a maximum overlap of fingerprints of 0.54 when  $\alpha \neq \beta$ . Hence, we obtain the experimental one-side error 0.77, while the theoretical one-side error is  $\frac{1+\delta^2}{2} = 0.75$ . The error probability is 1 for any classical one-bit fingerprinting with one-sided error.

The observable errors in the experiment come from pulse imperfections, both in the TSE and spin selective pulses, variability over time of the measurement process, and RF field inhomogeneity. Since the  $T_2$  relaxation times of the spins varied from 0.42 – 0.8s compared to the experiment duration of 0.23s, the net loss of magnetization due to relaxation is not negligible. This effect have been reduced by renormalizing the integration of the spectra during the measurement stage.

In conclusion, we have used a three-spin system and liquid-state NMR to demonstrate a proof-in-principle

quantum device, and we also test several potential applications in quantum information, both quantum computation and quantum communication complexity, in this single quantum device. The implemented quantum circuit forms the basis for many interesting and quantum information tasks. The experimental results show good agreement with the theoretical predictions.

*Note added.* After completing this work, it has come to our knowledge that Rolf T. Horn *et al.* [21] have demonstrated the single-qubit quantum fingerprinting using linear optics.

This project was supported by Temasek Project in Quantum Information Technology (Grant No. R-144-000-071-305). We also thank supports from the National Nature Science Foundation of China (Grant No. 10075041), Funded by the National Fundamental Research Program (2001CB309300) and National Science Fund for Distinguished Young Scholars (Grant No. 10425524). DKLO acknowledges support from EU grants RESQ (IST-2001-37559) and TOPQIP (IST-2001-39215), Fujitsu, and Sidney Sussex College Cambridge.

- 
- [1] A. Y. Kitaev, quant-ph/9511026.  
 [2] R. Cleve and A. Ekert, C. Macchiavello, and M. Mosca, Proc. R. Soc. Lond. A **454**, 339 (1998).  
 [3] D. Abraham and S. Lloyd, Phys. Rev. Lett. **83**, 5162 (1999).  
 [4] C. Miquel, J. P. Paz, M. Saraceno, E. Knill, R. Laflamme and C. Negrevergne, Nature (London) **418**, 59 (2002).  
 [5] H. Buhrman, R. Cleve, J. Watrous and R. D. Wolf, Phys. Rev. Lett. **87**, 167902 (2001).  
 [6] A. Ekert et. al., Phys. Rev. Lett. **88**, 217901 (2002).  
 [7] P. Horodecki and A. Ekert, Phys. Rev. Lett. **89**, 127902 (2002).  
 [8] Lieven M.K. Vandersypen and Isaac L. Chuang, quant-ph/0404064 (to appear in Rev. Mod. Phys. 4th October 2004).  
 [9] J. Niel de beaudrap, Phys. Rev. A **69**, 022307 (2004).  
 [10] D. G. Cory, A. F. Fahmy, and M. D. Price, Physica (Amsterdam) **120D**, 82 (1998).  
 [11] J. Du et al., Phys. Rev. Lett. **91**, 100403 (2003).  
 [12] E. Fredkin and T. Toffoli, J. Theoret. Phys. **21**, 219 (1982).  
 [13] A. Barenco et. al., Phys. Rev. A **52**, 3457 (1995).  
 [14] H. F. Chau and F. Wilczek, Phys. Rev. Lett. **75**, 748 (1995).  
 [15] J. A. Smolin and D. P. Divincenzo, Phys. Rev. Lett. **53**, 2855 (1996).  
 [16] J. Du et al., Phys. Rev. A **63**, 042302 (2001).  
 [17] F. Xue et al. Chin. Phys. Lett. **19**, 1048 (2002).  
 [18] X. Peng et al., J. Chem. Phys. **120**, 3579 (2004).  
 [19] S. Massar, quant-ph/0305112.  
 [20] A. Uhlmann, Rep.Math. Phys. **9**, 273 (1976)  
 [21] Rolf T. Horn et al., quant-ph/0410232.